Supporting Information

Controlled Growth of Large-scale Uniform 1T′ $MoTe_2$ Crystals with Tunable Thickness and Its Photodetector Application

Xiaojian Wang[a, b], Jing Shang[c, d], Meijie Zhu[b], Xi Zhou[a], Rui Hao[a], Lina Sun[a], Hua Xu[e], Jianbang Zheng*[b], Xingfeng Lei[a], Chun Li[d], Liangzhi Kou*[c], Qingliang Feng*[a]

a. Key Laboratory of Special Functional and Smart Polymer Materials of Ministry of Industry and Information Technology, School of Chemistry and Chemical Engineering, Northwestern Polytechnical University, Xi'an 710072, P. R. China
Email: fengql@nwpu.edu.cn.
b. MOE Key Laboratory of Material Physics and Chemistry under Extraordinary Conditions, School of Science, Northwestern Polytechnical University, Xi'an 710072, P. R. China
E-mail: zhengjianbang@nwpu.edu.cn
c. School of Chemistry, Physics and Mechanical Engineering Faculty, Queensland University of Technology, Garden Point Campus, QLD 4001, Brisbane, Australia
E-mail: liangzhi.kou@qut.edu.au
d. Department of Engineering Mechanics, Northwestern Polytechnical University, Xi'an 710072, China
e. School of Materials Science and Engineering, Shaanxi Normal University, Xi'an 710119, P. R. China

Structure and composition Characterization: Optical images are taken on an Olympus BX51 microscope. AFM is done on a Bruker ICON microscope. XPS analysis is done on an Axis Ultra system. TEM imaging was performed on a probe aberration-corrected JEM-2100F operated at 200 kV. Normal Raman are measured on a Renishaw in Via micro-Raman spectroscope with 532 nm laser. Angle-resolved polarization Raman spectra are achieved with a half-wave being used to turn the polarization angle of excitation laser. The angular optical contrast spectrum is obtained using a Witec RSA300+ confocal optical microscope equipped with a 100× objective (N.A.= 0.9). The angle-resolved optical contrast is performed with polarized light from a KL 1500 halogen lamp (Zeiss) by rotating the samples. Angle -resolved polarized optical image is captured by adding a polarizer in the light path of the optical microscope.

Device Fabrication and Electrical Measurement: The few-layer 1T′ $MoTe_2$ Crystal devices are fabricated by electron-beam lithography and physical mask with Cu grid, and the contact metal of Cr/Au (5/50 nm) electrodes are fabricated by thermal evaporation deposition. The measurement is carried out in a probe station and measured by Keithley 2614b semiconductor analyzer under ambient air at room temperature. Wavelength-dependent photo-response of the devices are performed under the 532 nm, 950 nm, and 1550 nm laser (power: 50 mW; focusing at the interface region with a diameter of ≈ 2 mm) excitation. Temperature-dependent I_{ds}-V_{ds} curves are performed on a heating stage.

Density-functional ab initial molecular dynamics (AIMD) simulations: The density-functional ab initial molecular dynamics (AIMD)[1] simulations have been performed on all structures by using the Vienna Ab initio simulation (VASP)[2] package, implemented with the generalized gradient approximation (GGA)[3]. All calculations employed Γ-point sampling of the Brillouin zone. In the present AIMD simulations, *NVT* canonical ensemble was performed by integrating the equations of motion at 1 fs time intervals, and controlling temperature via a Nosé-Hoover thermostat that the temperature ranges from 300 to 1100 K with a step of 200 K. At each of time step, the total energy was convergent to an accuracy of 10^{-4} eV/atom using a plane-wave energy cutoff of 400 eV. The total simulation time was 3000 ps at every temperature. The atomic-scale AIMD 4 × 4 × 1 supercell model of 1T' $MoTe_2$ nanoribbons with 96 atoms are constructed.

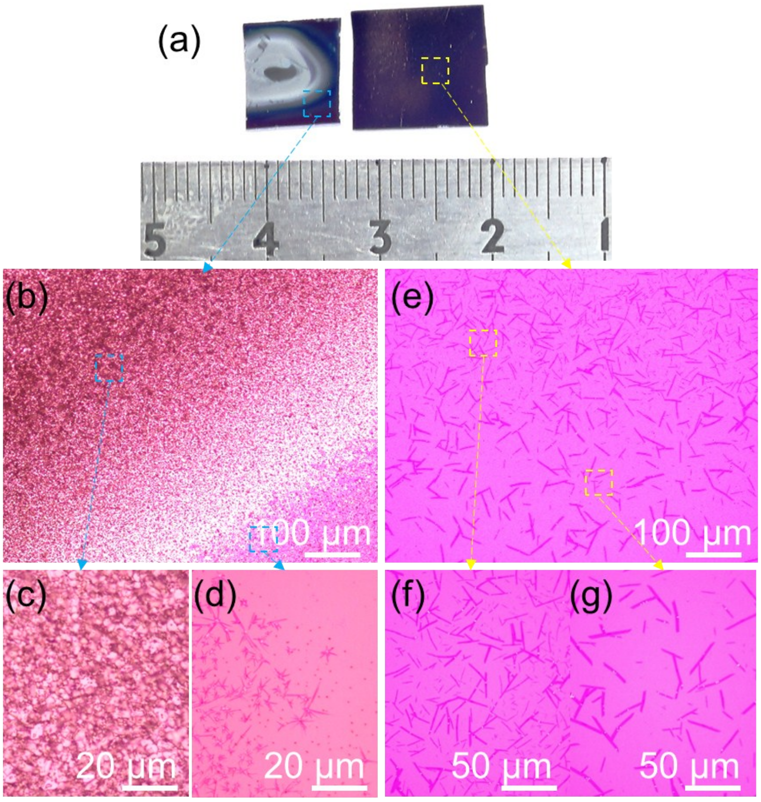

Figure S1. Compared experimental result for normal and modified CVD growth of 1T′ $MoTe_2$. (a) The photograph of substrate for 1T′ $MoTe_2$ growth with (right) and without (left) molecular sieve assistant. (b-d) Optical images of normal CVD growth of 1T′ $MoTe_2$ in large scale, center and the edge of substrate, respectively. (e-g) Optical images of modified CVD growth of 1T′ $MoTe_2$ in large scale, center and the edge of substrate, respectively.

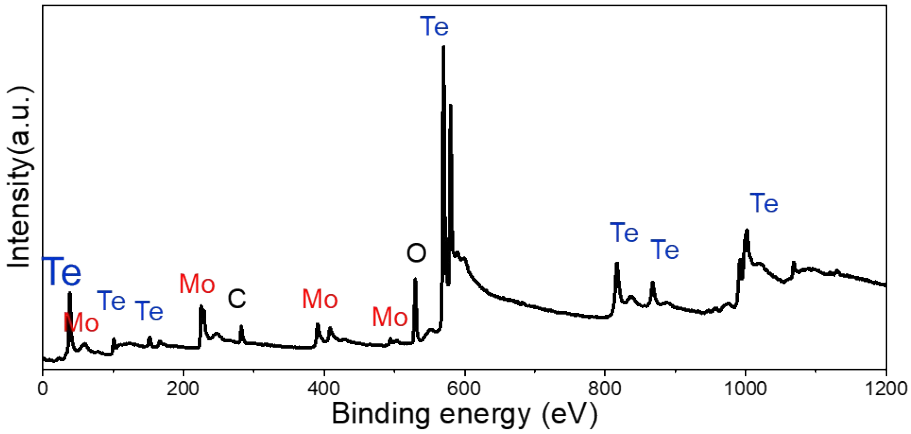

Figure S2. XPS full spectrum of single crystal 1T′ $MoTe_2$ on SiO_2/Si substrate.

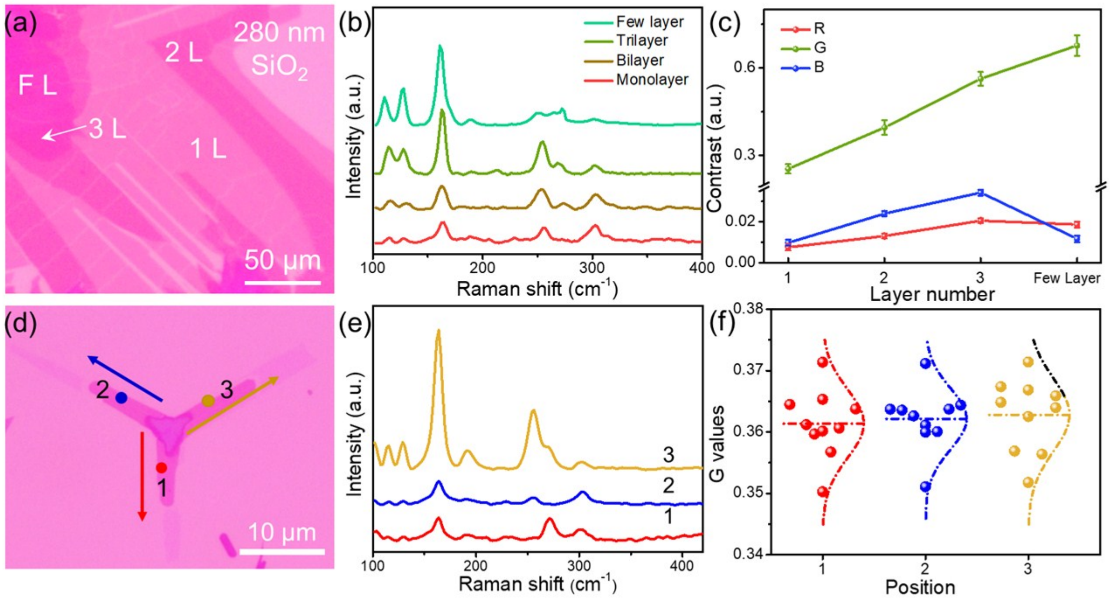

Figure S3. (a) Optical microscopy image of transfered monolayer, bilayer and trilayer of 1T′ $MoTe_2$ on SiO_2/Si substrate with 300 thickness oxide layer. (b) Raman spectra of 1T′ $MoTe_2$ in different layers. (c) The relationship between the optical contrast of R, G, and B channels of 1T′ $MoTe_2$ and layer numbers on 300 nm SiO_2/Si. (d) A selected sample of 1T′ $MoTe_2$ with a special morphology. (e,f) Raman spectra and the G value of optical contrast at three positions in Figure S3d.

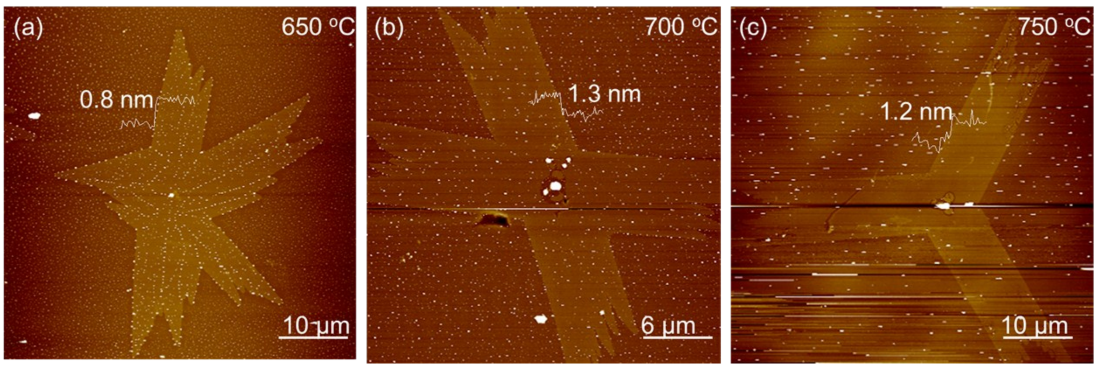

Figure S4. (a-b) AFM images of monolayer (a), bilayer (b-c) 1T′ $MoTe_2$ crystal are obtained at 650 °C, 700 °C, and 750 °C, respectively.

Table S1: Figure-of-merit of photosensing devices based on some other typical 2D materials.

Materials	Spectral range[nm]	R [AW^{-1}]	Response time [ms]	Ref.
GaS	254–610	19.2	≤30	4
MoS_2	300-800	1.96	98	5
WSe_2	500–900	1.8×10^5	5×10^3	6
InSe	370–980	27	500	7
GaSe	254–610	2.8	20	8
In_2Se_3	254–1064	20.5	24.6	9
BP	400–940	4.8×10^{-3}	1	10
2H $MoTe_2$	600-1750	0.05	1.6	11
Thick 1T′ $MoTe_2$	532-10600	0.4×10^{-3}	42.5×10^{-3}	12
Few layer 1T′ $MoTe_2$	532-1550	0.83	5×10^3	This work

Reference:

1 R. Car and M. Parrinello, Unified Approach for Molecular Dynamics and Density-Functional Theory. *Phys. Rev. Lett. 55, 2471 (1985).*

2 G. Kresse and J. Furthmüller, Efficient iterative schemes for ab initio total-energy calculations using a plane-wave basis set. *Phys. Rev. B 54 11169 (1996).*

3 J. P. Perdew, K. Burke, and M. Ernzerhof, Generalized Gradient Approximation Made Simple. *Phys. Rev. Lett. 77 3865 (1996).*

4 P. Hu, L. Wang, M. Yoon, J. Zhang, W. Feng, X. Wang, Z. Wen, J. C. Idrobo, Y. Miyamoto, D. B. Geohegan, K. Xiao, *Nano Lett*. 2013, **13**, 1649.

5 L. Jiao, W. Jie, Z. Yang, Y. Wang, Z. Chen, X. Zhang, W. Tang, Z. Wu, J. Hao, *J. Mater. Chem. C*. 2019, **7**, 2522-2529.

6 W. Zhang, M.-H. Chiu, C.-H. Chen, W. Chen, L.-J. Li, A. T. S. Wee, *ACS Nano.* 2014, **8**, 8653.

7 Z. Yang, W. Jie, C.-H. Mak, S. Lin, H. Lin, X. Yang, F. Yan, S. P. Lau, J. Hao, *ACS Nano.* 2017, **11**, 4225.

8 P. Hu, Z. Wen, L. Wang, P. Tan, K. Xiao, *ACS Nano.* 2012, **6**, 5988.

9 Z. Q. Zheng, J. D. Yao, G. W. Yang, *J. Mater. Chem. C.* 2016, **4**, 8094.

10 M. Buscema, D. J. Groenendijk, S. I. Blanter, G. A. Steele, H. S. J. van der Zant, A. Castellanos-Gomez, *Nano Lett*. 2014, **14**, 3347.

11 H. Huang, J. Wang, W. Hu, L. Liao, P. Wang, X. Wang, F. Gong, Y. Chen, G. Wu, W. Luo, H. Shen, T. Lin, J. Sun, X. Meng, X. Chen, J. Chu, *Nanotechnology.* 2016, **27**, 445201.

12 J. Lai, X. Liu, J. Ma, Q. Wang, K. Zhang, X. Ren, Y. Liu, Q. Gu, X. Zhuo, W. Lu, Y. Wu, Y. Li, J. Feng, S. Zhou, J.-H. Chen, D. Sun, *Adv. Mater*. 2018, **30**, 1707152.